Optics Communications 283 (2010) 4892–4898

Contents lists available at ScienceDirect

Optics Communications

journal homepage: www.elsevier.com/locate/optcom

Quasi Bessel beam by Billet's *N*-split lens

Chieh-Jen Cheng, Jyh-Long Chern *

Department of Photonics, Institute of Electro-Optical Engineering, National Chiao Tung University, Hsinchu 300, Taiwan, ROC

ARTICLE INFO

Article history:
Received 18 May 2010
Received in revised form 8 July 2010
Accepted 27 July 2010

Keywords:
Diffraction
Paraxial wave optics
Billet's split lens
Bessel beam

ABSTRACT

This study utilizes the focal property of a classical Billet's split lens to create more focal points by splitting the lens. This approach distributes the focal points circularly on the focal plane. This study explores the characteristics of beam propagation and analytically derives the asymptotic characteristics of beam propagation based on the stationary phase approximation and the moment-free Filon-type method. Results show that the unique Billet's *N*-split lens can generate a quasi Bessel beam if the number of splitting *N* is large enough, e.g., $N \geqq 24$. This study also explores the diffraction efficiency of corresponding quasi Bessel beam and the influence of aperture size. The potential advantage of proposed split lens approach is that, unlike the classical means of annular aperture, this simple lens approach allows a much larger throughput in creating the Bessel beam and hence the Bessel beam could have more optical energy.

1. Introduction

Field propagation and its associated diffraction behavior are fascinating and is a classical topic in optical research [1]. Diffraction and field propagation have many applications in optical testing [2] and the development of new optical devices associated with nanotechnology [3]. For product development and practical applications, the current optical product design is still essentially based on ray optics, while diffraction-based theory generally provides a reference for performance limitations and baseline of resolution. Nevertheless, the study of diffraction theory in optical fields remains an important topic. Recent advances in the literature include the selected works of E. Wolf [4]. To meet the demand of technology development and academic interest, our early study explored far-field behavior with sub-wavelength variations in which aperture (stop) plays a key role in information retrieval [5]. Previous research indicates that an aperture stop (circular and rectangular) and a perfect lens are established platforms for exploring diffraction behavior. Investigations on this topic generally fall into one of two categories:

(1) light beams could be different, with polarized or vector formalism;
(2) the lenses may contain aberrations, e.g., spherical aberration or coma.

However, it is possible to adopt a different approach. This study considers the generalization of a conventional perfect lens with split surface profile. Lens splitting can be implemented in many different ways, such as a configuration of Meslin's experiment or Billet's split lens [6]. Once a lens is split in multiple pieces, the resulting interference will involve multiple beams and the configuration of multiple paths, creating a relatively complex situation for beam propagation and interference. *Is it possible to have simple beam characteristics with such a complex configuration?* Furthermore, *could we have a different means of controlling the beam characteristics?*

The answers to the issues above could be very constructive. If we consider the disturbance of the focal points with these split lenses, i.e., either the Meslin or Billet design, the complexity could be greatly simplified. This is because the focal points are located in a plane normal to the optical axis in Billit's configuration, and distributed along the optical axis for Meslin's configuration [6]. Both of these configurations provide a simple means of confining the focal points vertically or horizontally and hence, give us a basis of the first-order optics for the analysis of beam propagation. This study presents the results of a generalized Billet's split lens, paying special attention to beam propagation. The generalization is implemented by splitting the lens further, i.e., by creating more focal points on the focal plane by distributing them circularly. The phenomena of field disturbance and propagation associated with such a generalized split lens are quite complicated. Our previous study explores the underlying symmetry properties of these phenomena [7]. Note that a Billet's split lens has already been developed for multiple imaging and multichannel optical processing [8]. This study shows that a *non-diffracting* Bessel beam [9] can be achieved by the use of such a split lens.

The Bessel beam is novel because of its propagation invariant since Durnin et al. [9] first reported the non-diffracting Bessel beam generated by an annular aperture [10]. The non-diffracting Bessel beams can also be generated by a phase optical element [11]. In additional to Bessel beam, the non-diffracting Mathiue-Gauss and

* Corresponding author. Tel.: +886 3 5712121x56348.
E-mail addresses: cjcheng.eo92g@nctu.edu.tw (C.-J. Cheng), jlchern@faculty.nctu.edu.tw (J.-L. Chern).

0030-4018/$ – see front matter © 2010 Elsevier B.V. All rights reserved.
doi:10.1016/j.optcom.2010.07.072

parabolic Gauss beams are introduced by Gutierrez-Vega et al. [12]. Moreover, the non-diffracting beam with mosaic pattern can be created by an apertured axicon [13] and the non-diffracting vortex beams have been studied by using an annular ring mask [14] or by focusing an array of laser arranged in a ring [15]. The width of annular aperture has to be small to produce a non-diffracting beam of long range [16,17] and hence, the energy loss is large. Diffractive optical element can generate an array of arbitrary focuses [18,19] and it is utilized as optical tweezers to trap and arrange particles in a particular shape [20,21], but it usually requires a complicated iterative calculation to obtain the phase/amplitude function. The advantage of the split lens approach is that, unlike the annual aperture, this simple lens approach allows a much more throughput in creating the Bessel beam and hence the Bessel beam has more optical energy.

2. Theoretical formalism

To illustrate the feature analytically, first consider a conventional focusing lens that is split into two identical halves (two sectors), where the upper half and lower half are moved a distance d up and down the Y-axis, respectively. This is the classical form of the Billet's split lens [6] schematically depicted in Fig. 1(a). This spilt lens produces a collimated uniform monochromatic wave of wavelength λ at two different foci, F_1 and F_2, in the focal plane. The diffraction theory employed here assumes that the aperture radius $a>>\lambda$, the focal

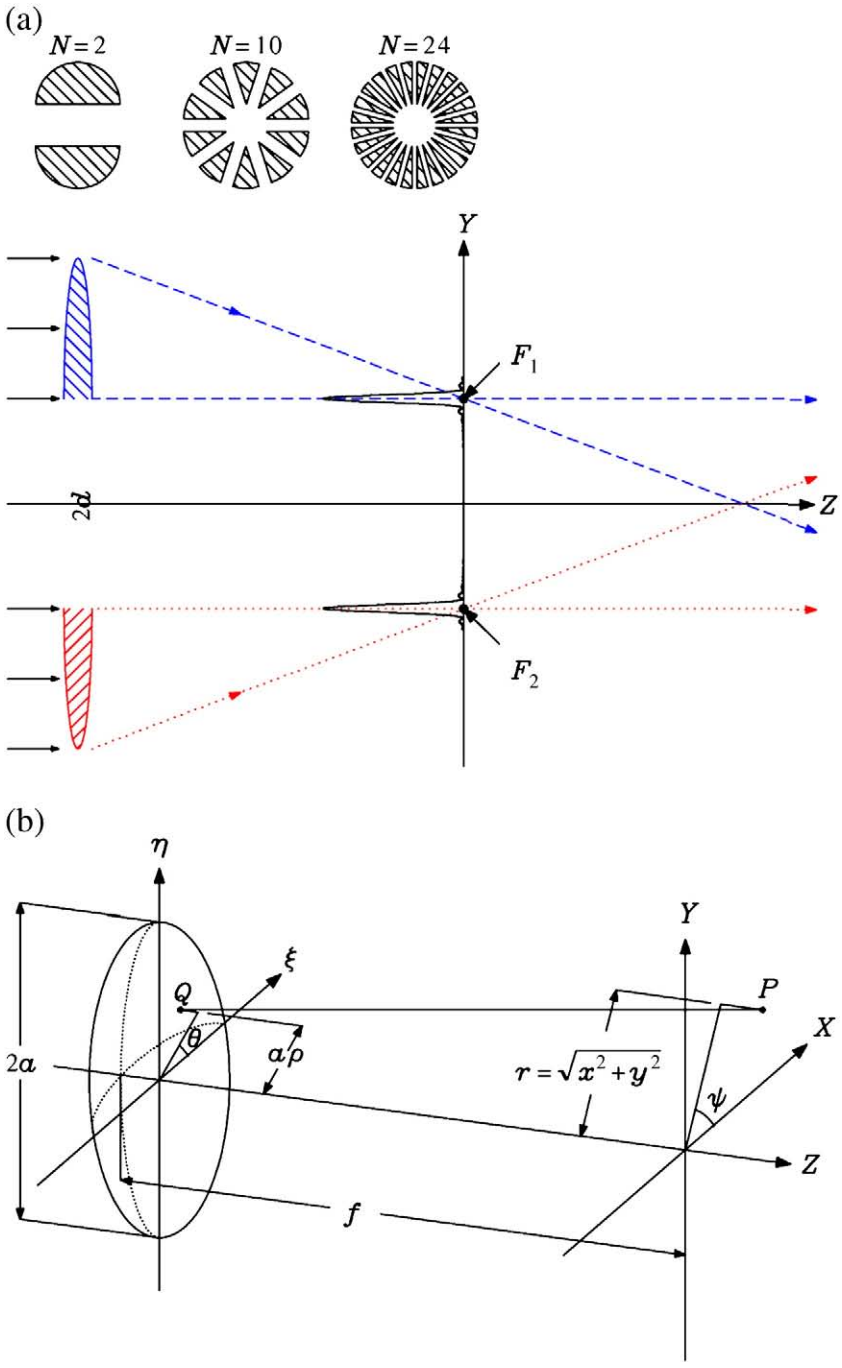

Fig. 1. (a) Schematic diagram of the Billet's split bisector lens. F_1 and F_2 are the first focus and second focus, respectively, and $2d$ is the separation distance between the foci of the two sectors. A front view on the left side shows the arrangement of sectors with $N=2$, 10, and 24, where N is the number of sectors. (b) Notation representation of the coordinate system of beam propagation.

length $f>>a>>\lambda$, and the Fresnel number $F=a^2/\lambda f$ is much larger than unity. When the (half) translation length d is zero, the two foci will coincide and the integral representation of the disturbance $U(P)$ at a point $P(x,y,z)$ in the image space is [6]

$$U(P) = -\frac{i}{\lambda}\frac{a^2 A}{f^2} e^{i\left(\frac{f}{a}\right)^2 u} \int_0^1 \int_0^{2\pi} e^{-i\left[v\rho\cos(\theta-\psi)+\frac{1}{2}u\rho^2\right]} \rho d\rho d\theta, \tag{1}$$

where A is the amplitude. The optical units $u = \frac{2\pi}{\lambda}\frac{a^2}{f^2}z$ and $v = \frac{2\pi}{\lambda}\left(\frac{a}{f}\right)r = \frac{2\pi}{\lambda}\left(\frac{a}{f}\right)\sqrt{x^2+y^2}$, denote the Cartesian coordinate position of $P(x, y, z)$ where $x = r\cos\psi$ and $y = r\sin\psi$. Fig. 1(b) shows the coordinate system. The disturbance $U(P)$ is

$$U(P) = C\int_0^1 e^{-i\frac{1}{2}u\rho^2} \int_0^{2\pi} e^{-i\left[\frac{2\pi a}{\lambda f}\rho(x\cos\theta + y\sin\theta)\right]} d\theta\rho d\rho, \tag{2}$$

where $C = -\frac{i}{\lambda}\frac{a^2 A}{f^2} e^{i\left(\frac{f}{a}\right)^2 u}$.

There are many different ways to split a lens. The example in this study divides the focusing lens into N equiangular sectors, and explodes and translates each sector at distance d in the r direction along the perpendicular bisector of the angle. Fig. 1(a) shows the schematic layouts of the cases of $N=2$, 10, and 24 on the top of Fig. 1. As a result of the ray-based analysis, the foci of all sectors form a regular N-sided polygon on the focal plane. Therefore, the focal point of each sector is

$$\begin{aligned} x_m &= d\cos\psi_m, \\ y_m &= d\sin\psi_m, \\ \psi_m &= \frac{2\pi}{N}(m+1/2), \quad m = 0,1,..,N-1. \end{aligned} \tag{3}$$

After applying coordinate translation and summing the contributions of all sectors, the disturbance $U(P)$ follows

$$U(P) = C\int_0^1 e^{-i\frac{1}{2}u\rho^2} \sum_{m=0}^{N-1} \int_{m\frac{2\pi}{N}}^{(m+1)\frac{2\pi}{N}} e^{-i\left[\frac{2\pi a}{\lambda f}\rho[(x-x_m)\cos\theta + (y-y_m)\sin\theta]\right]} d\theta\rho d\rho. \tag{4}$$

Substituting Eq. (3) into Eq. (4) leads to

$$U(P) = C\int_0^1 e^{-i\frac{1}{2}u\rho^2} \sum_{m=0}^{n-1} \int_{m\frac{2\pi}{N}}^{(m+1)\frac{2\pi}{N}} e^{-i\left\{\frac{2\pi a}{\lambda f}\rho[r\cos(\theta-\psi)-d\cos(\theta-\psi_m)]\right\}} d\theta\rho d\rho. \tag{5}$$

After setting the interval of integration for each segment to the same value, the term d in the brackets of exponential function is no longer a function of m. The summation is rewritten,

$$U(P) = C\int_0^1 e^{-i\frac{1}{2}u\rho^2} \int_0^{\frac{2\pi}{N}} e^{iv_d\rho\cos\left(\theta-\frac{\pi}{N}\right)} \times \sum_{m=0}^{N-1} e^{-iv\rho\cos\left(\theta-\psi+m\frac{2\pi}{N}\right)} d\theta\rho d\rho, \tag{6}$$

where $v_d = \frac{2\pi}{\lambda}\left(\frac{a}{f}\right)d$. If the sector number N is large, ψ_m is approximately equal to θ and the disturbance can be reduced

$$U(P) = C\int_0^1 e^{-i\left(\frac{1}{2}u\rho^2 - v_d\rho\right)} \int_0^{\frac{2\pi}{N}} \sum_{m=0}^{N-1} e^{-iv\rho\cos\left(\theta-\psi+m\frac{2\pi}{N}\right)} d\theta\rho d\rho. \tag{7}$$

The azimuthal integration can be done by the zero-order Bessel function of the first kind J_0 and the disturbance takes the form

$$U(P) = 2\pi C\int_0^1 J_0(v\rho) e^{-i\left(\frac{1}{2}u\rho^2 - v_d\rho\right)} \rho d\rho. \tag{8}$$

The following discussion uses the stationary phase approximation to evaluate the disturbance *when z is much larger than* d/NA, where NA is the numerical aperture. This leads to

$$U(P) = -\frac{2\pi i a^2 A}{\lambda f^2} e^{i\left(\frac{f}{a}\right)^2 u} \sqrt{\frac{2\pi}{u}} e^{-\frac{\pi i}{4}} J_0\left(v\frac{v_d}{u}\right)\frac{v_d}{u} e^{i\frac{v_d^2}{2u}}. \tag{9}$$

The amplitude can be written as

$$|U(P)| = \frac{2\pi a^2 A}{\lambda f^2}\sqrt{\frac{2\pi}{|u|}} J_0\left(v\frac{v_d}{u}\right)\frac{v_d}{u}. \tag{10}$$

When z is smaller than d/NA, use the moment-free Filon-type method [22] or integration by parts to evaluate the asymptotic approximation of Eq. (8) with an error of order $O(v_d^{-2})$. This leads to

$$U(P) = -\frac{2\pi C i}{v_d - u} e^{i\left(v_d - \frac{u}{2}\right)} J_0(v), \tag{11}$$

and the amplitude is

$$|U(P)| = \frac{2\pi}{\lambda}\frac{a^2 A}{f^2}\frac{J_0(v)}{v_d - u}, \tag{12}$$

Eqs. (10) and (12) show that the amplitude in the radial direction near the optical axis is a J_0 Bessel function. This profile is not a function of u, and is collimated when the propagation distance z is smaller than d/NA, and, conversely, the profile of J_0 Bessel is a function of u^{-1} and the beam propagates when z exceeds d/NA.

3. Numerical identification

This section numerically verifies the feature described above. To meet the diffraction beam requirements, i.e., the numerical aperture (NA) should be small (around 0.05), take a typical lens with a focal length of a few 10 mm, e.g., $f=80{,}000\lambda$, such that the aperture radius $a=4000\lambda$. Then set the (half) separation distance $d=1000\lambda$. For the numerical example of $\lambda=630$ nm, we have $f=50.4$ mm, $a=2.52$ mm, and $d=0.63$ mm.

Fig. 2(a) illustrates the intensity disturbance in the XY-plane of $z=0$, which is the focal plane, for the case of $N=10$, while Fig. 2(b) illustrates that for $N=24$. The plots of intensity disturbance in Fig. 2 are normalized to 100. Fig. 2(a) shows that there are ten focal spots along the azimuthal direction because the number of sectors N is ten. These ten spots form ten vertexes that resemble a regular ten-sided polygon, where the circumscribed radius is $d=1000\lambda$ and the center is at the origin. On the other hand, when the number of sectors increases, e.g., $N=24$, there are twenty four focal spots resembling a better annular ring pattern with the circumscribed radius of 1000λ in the focal plane, as Fig. 2(b) shows. The annular ring pattern is similar to an annular slit, and the width of the slit is based on the numerical aperture of the Billet's N-split lens. Compared with these focal spots, the intensity near the optical axis is too dim to observe the Bessel profile in Fig. 2.

Next, consider the intensity disturbance in the meridional plane with $\psi=0$ (XZ-plane). Fig. 3(a) and (b) illustrates the cases of $N=10$ and 24, respectively. These figures reveal a quasi Bessel beam profile beyond $z=d$/NA, particularly for $N=24$, which is essentially caused by the ring-like pattern forming on the focal plane. The intensity maximum is not located on the focal plane, but located approximately at $z=d$/NA instead. The location of maximum z_{max} can be numerically evaluated to be $22{,}187\lambda$ and $22{,}421\lambda$ when $N=10$ and 24, respectively.

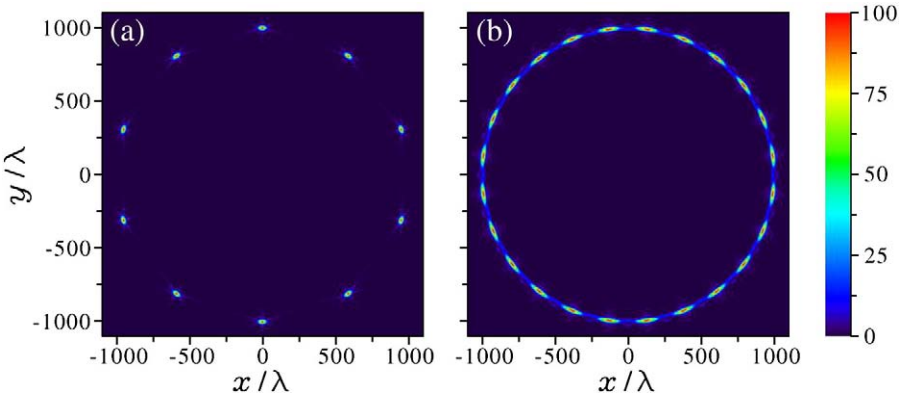

Fig. 2. Normalized intensity disturbance of the generalized N-split lens in the focal plane, where (a) $N=10$ and (b) $N=24$.

4. Asymptotic behavior

In this section, we study the asymptotic behavior of the radial intensity disturbance along the Z-axis at $z=0$, 10,000λ, z_{max}, 40,000λ, 60,000λ and 80,000λ are shown in Fig. 3(c) and (d) for $N=10$ and 24, respectively. Note that the radial intensity within $z=d/\mathrm{NA}$ has been multiplied by 100, as the plots and the regions of illustration are not the same. Note that the asymptotic result calculated by the stationary phase approximation is for $z>>d/\mathrm{NA}$, while on the other hand, for $z<d/\mathrm{NA}$. This result is based on the moment-free Filon-type method. Fig. 3(c) and (d) shows the asymptotic forms with dark lines. Note that the error between the calculated intensity and the asymptotic expression based on moment-free Filon-type method is already enlarged by 100.

To indicate the beam propagation characteristics of quasi J_0 Bessel, Fig. 3(c) and (d) plots the first three roots of J_0 Bessel function parallel to the optical axis. These three roots denote the first three dark rings of quasi Bessel beam in Eq. (12). Eq. (12) predicts that the J_0 Bessel function is not a function of z, i.e., the quasi Bessel beam near the optical axis is collimated within $z=d/\mathrm{NA}$ and the intensity is inversely proportional to $(v_d-u)^2$. Indeed, the on-axis intensity increases from the focal plane and reaches its maximum intensity when $u=v_d$. On

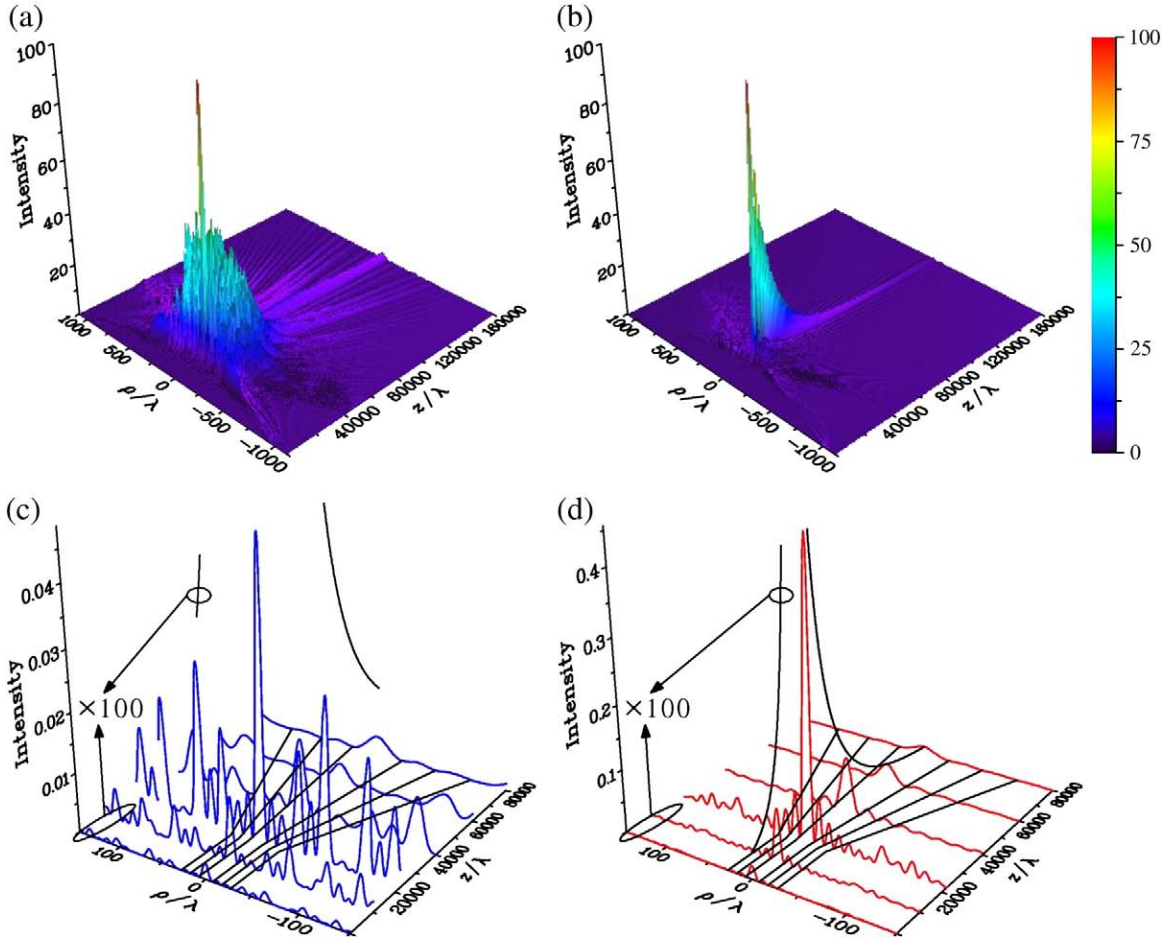

Fig. 3. The intensity disturbances in the meridional plane with $\psi=0$ (XZ-plane) for the different number of split sectors, (a) $N=10$ and (b), $N=24$, where the intensity is normalized to 100. Plots with enlarged scale are shown in (c), $N=10$, and (d), $N=24$, where the first three dark rings of the J_0 are illustrated at the bottom. The on-axis intensity of asymptotic approximations is denoted with solid lines. The intensity within $z=d/\mathrm{NA}$ has been multiplied by 100 as denoted by a circle in the plots (see text).

the other hand, Eq. (10) indicates that the on-axis intensity beyond $z = d/\mathrm{NA}$ decays because the intensity is inversely proportional to $u^{3/2}$. The variable in the J_0 Bessel function is $v\frac{v_d}{u}$. Hence, the locations of minimum in the J_0 Bessel function are linearly proportional to z and can be plotted as straight lines with slopes of $\frac{j_k}{d\cdot 2\pi/\lambda}$, where j_k are the roots of J_0 Bessel function [9].

Fig. 3(c) and (d) plots the first three straight lines. In the case of $N = 10$, three dark rings of Bessel profile are apparently near $z = d/\mathrm{NA}$. On the other hand, there are eight dark rings when $N = 24$. Except for z, which is near d/NA, these lines fit the dark rings, and present the propagation properties of J_0 Bessel beam clearly.

5. Influence of aperture size

To discuss the influence of aperture size, i.e., the radius a, on the diverging J_0 Bessel beam, we calculate the intensity disturbance in the meridional plane with the number of split sectors $N = 24$ and $\psi = 0$ (XZ-plane) for different aperture radius $a = 40{,}000\lambda$, $24{,}000\lambda$ and $16{,}000\lambda$. In Fig. 4 in which the dimension is in a logarithmic scale, we use the linear curves to denote the dark rings of the J_0 Bessel beam. All intensities in the frames are normalized by the maximum intensity as the aperture radius $a = 40{,}000\lambda$. The asymptotic approximation tells the argument in the diverging J_0 Bessel function is $v\frac{v_d}{u}$, or $\frac{2\pi}{\lambda}d\frac{r}{z}$ where there is no aperture radius a in this argument. In other words, the diverging J_0 Bessel beam is related to the z and r directly, instead of the aperture radius a. However, the diverging J_0 Bessel beam is starting from $z = d/\mathrm{NA} = f\cdot d/a$. The aperture radius a, therefore, determines the position of the diverging J_0 Bessel beam and controls the beam radius of J_0 Bessel beam via $z = d/\mathrm{NA}$. As shown in Fig. 4, different aperture sizes result in different location of $z = d/\mathrm{NA}$ and give rise to a minimum beam radius at $z = d/\mathrm{NA}$. Consequently, a larger aperture radius, having larger focusing power, leads to a smaller beam radius at $z = d/\mathrm{NA}$, location of the minimum beam radius.

Fig. 5 illustrates the intensity disturbance in the meridional plane using the same parameters as in Fig. 4 except that the azimuthal angle $\psi = \pi/24$. The J_0 Bessel beams in Figs. 4 and 5 are similar within the seventh dark ring, but they become different once away from the seventh dark ring. The difference of intensity disturbance is resulted from the foci of split sectors. In our arrangement, there are two foci contributing to the J_0 Bessel beam in the meridional plane with $\psi = \pi/24$. However, there is no focus in the XZ-plane and it gives rise to the J_0 Bessel beam having different intensity disturbance from that in the meridional plane with $\psi = \pi/24$. As already shown in Fig. 2, different intensity disturbance along different azimuthal angle occurs because of the arrangement of the sectors.

The on-axis intensity with the number of split sectors $N = 24$ is shown in Fig. 6 for different aperture sizes, i.e., $a = 40{,}000\lambda$, $32{,}000\lambda$, $24{,}000\lambda$, $16{,}000\lambda$ and 8000λ. It is to reflect the influence of aperture size on the diverging J_0 Bessel beam. The inset shows the on-axis intensity with a logarithmic scale. All the intensities in Fig. 6 are normalized by the maximum intensity as the aperture radius $a = 40{,}000\lambda$. We can readily see that all the asymptotes of oscillating curves overlap when z is beyond d/NA. The inset with a logarithmic scale shows clearly the overlapping of the on-axis intensity with different aperture radius.

In short, the aperture size determines the ranges of the asymptotic solution of the J_0 Bessel beam generated by the Billet's N-split lens. Moreover, a larger aperture radius, having larger focusing power, leads to a larger maximum on-axis intensity near $z = d/\mathrm{NA}$. Note that the location of the maximum on-axis intensity is *close* to $z = d/\mathrm{NA}$, not really on $z = d/\mathrm{NA}$.

6. Conclusions

In conclusion, this study shows that it is possible to generate a quasi J_0 Bessel beam using a Billet's N-split lens that introduces a monochromatic plane wave to a ring-like pattern on the focal plane when N is large enough, e.g., 24. This study derives the asymptotic characteristics of beam propagation for the quasi J_0 Bessel beam from the stationary phase approximation and the moment-free Filon-type method.

Results show that the beam is collimated within $z = d/\mathrm{NA}$, i.e., the dark rings of the J_0 Bessel beam result in straight lines that are parallel to the optical axis. On the other hand, the beam begins to diverge as $z > d/\mathrm{NA}$, and the dark rings of J_0 Bessel beam lead to straight lines with

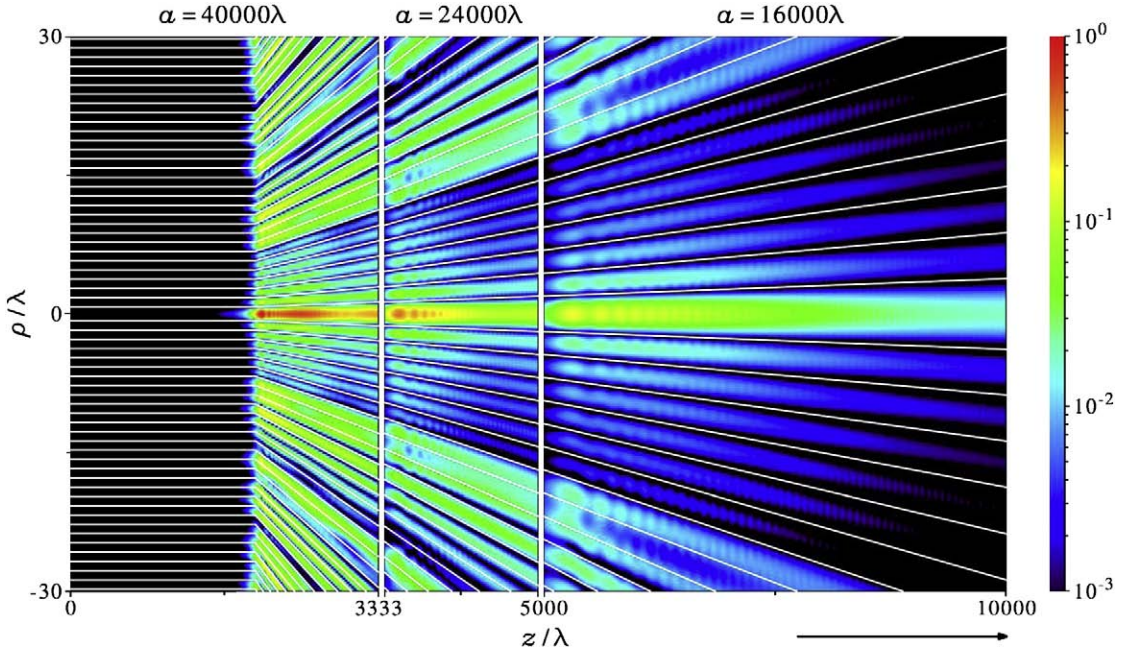

Fig. 4. The intensity disturbances in the meridional plane with the number of split sectors $N = 24$ and $\psi = 0$ (XZ-plane) for the aperture radius at $a = 40{,}000\lambda$, $24{,}000\lambda$ and $16{,}000\lambda$ which corresponds to NA = 0.5, 0.3 and 0.2, respectively. The intensity is normalized by the maximum intensity of the case with $a = 40{,}000\lambda$. The logarithmic scale is used here. The solid lines also illustrate the dark rings of the J_0 Bessel beam.

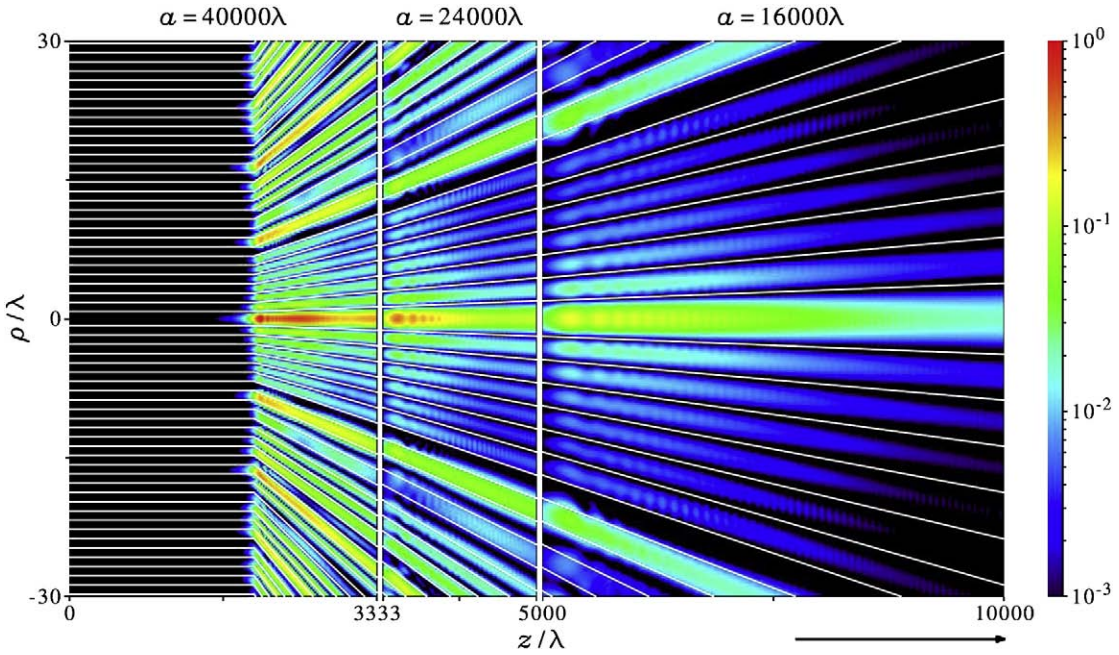

Fig. 5. The intensity disturbances in the meridional plane with the number of split sectors $N=24$. The parameters were the same as in Fig. 4 except that the azimuthal angle $\psi=\pi/24$.

intrinsically-determined slopes. Moreover, the oscillatory property of the on-axis intensity could be deduced, i.e., it increases from the focal plane to a maximum at $z\sim d/\mathrm{NA}$, while changed to oscillate downwardly as $z>d/\mathrm{NA}$. The aperture radius determines the location of d/NA and controls the minimum radius of J_0 Bessel beam. As expected, larger aperture radius result in smaller beam radius at $z=d/\mathrm{NA}$ and larger on-axis intensity near $z=d/\mathrm{NA}$ because of larger focusing power.

It is interesting to note the fraction of total energy encircled within a circle of radius v about the optical axis in the detecting XY-plane $u=$ constant. Table 1 shows the fraction of encircled energy within the third dark ring $v=v_{j3}=j_3\cdot u/v_d$ and the seventh dark ring $v=v_{j7}=j_7\cdot u/v_d$ for $N=10$, 24 and $N\to\infty$ at $u=2d/\mathrm{NA}=20{,}000\lambda$. As $N\to\infty$, there is 5.5% and 13.5% of total energy encircled within three dark rings and seven dark rings, respectively. If we place a second focal lens with a focal length f_2 such that the front focal plane of the second lens is the back focal plane of the first split lens [9]. The effective radius [16] on the second lens is $R_{\mathrm{eff}}=d\pm f_2\ \lambda/\Delta d\sim 20{,}516\lambda$ in our notation with $f_2=30$ cm and $\Delta d\sim 1.22\lambda/\mathrm{NA}\sim 24.4\lambda$. Noting that d is the radius instead of the diameter of the ring. The corresponding fraction of encircled energy within R_{eff} is now 81.68% as $N\to\infty$. The generation of quasi Bessel beam has a good utilization of incident energy. Noting that, the Bessel beam generated by a diffractive phase element can possess a high diffraction efficiency of up to 93.12% [19].

Finally, note that a segmented-aperture optical system in which phase-shifting material fills each segmented region [23,24] makes it possible to realize the generalized Billet's N-split lens and create a quasi Bessel beam. The phase-shifting material could be liquid crystal for this study. It is still worthwhile to highlight again that the benefit of current split lens approach is that, unlike the annual aperture, this simple lens approach allows a much large throughput in creating the Bessel beam and hence the Bessel beam could have more optical energy.

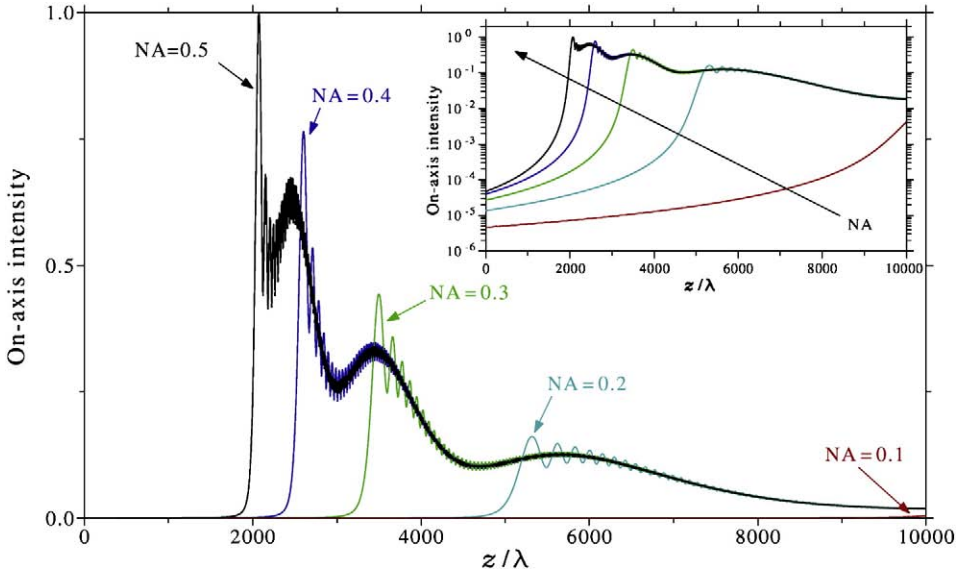

Fig. 6. The on-axis intensity for the aperture radius at $a=40{,}000\lambda$, $32{,}000\lambda$, $24{,}000\lambda$, $16{,}000\lambda$ and 8000λ which corresponds to NA = 0.5, 0.4, 0.3, 0.2 and 0.1, respectively. The intensity is normalized by the maximum on-axis intensity of the case with $a=40{,}000\lambda$. The inset displays the logarithmic scaling for the on-axis intensity.

Table 1
Fractions of energy at $z=2d/\mathrm{NA}$ for $N=10$, 24 and ∞, where the aperture radius $a=4000\lambda$.

	$N=10$	$N=24$	$N\to\infty$
v_{j3}	0.0069	0.0471	0.0550
v_{j7}	0.0449	0.1149	0.1353

Acknowledgement

We thank the referees for their comments and suggestions on the inclusions of the influence of aperture size, the discussion of diffraction efficiency, and the references of Bessel beam. This work is partially supported by the National Science Council, Taiwan, ROC, under project NSC-96-2628-E-009-019-MY3. Chieh-Jen Cheng and Jyh-Long Chern can be reached at cjcheng.eo92g@nctu.edu.tw and jlchern@faculty.nctu.edu.tw, respectively.

References

[1] M. Mansuripur, Classical Optics and its Applications, 2nd. Ed.Cambridge University Press, 2009.
[2] Optical Shop Testing, in: D. Malacara (Ed.), 3 rd. ed., Wiley Interscience, 2007.
[3] L. Novotny, B. Hecht, Principles of Nano-Optics, Cambridge University Press, 2006.
[4] E. Wolf, Selected works of E. Wolf, with commentary, World Scientific, 2001.
[5] S.-C. Chu, J.-L. Chern, Opt. Lett. 29 (2004) 1045;
J. Opt. Soc. Am. A 23 (2006) 2471;
Opt. Commun. 281 (2008) 1997.
[6] M. Born, E. Wolf, Principles of Optics, 7th expended ed.Cambridge University Press, 1999.
[7] C.-J. Cheng, J.-L. Chern, Opt. Commun. 283 (2010) 3564.
[8] A.S. Kumar, R.M. Vasu, Appl. Opt. 26 (1987) 5345.
[9] J. Durnin, J.J. Miceli Jr., J.H. Eberly, Phys. Rev. Lett. 58 (1987) 1499;
A review article could be found from. D. McGloin, K. Dholakia, Contemp. Phys. 46 (2005) 15.
[10] W.D. Montgomery, J. Opt. Soc. Am. 57 (1967) 772.
[11] V.V. Kotlyar, S.N. Khonina, V.A. Soifer, J. Mod. Opt. 42 (1995) 1231.
[12] J.C. Gutierrez-Vega, M.A. Bandres, J. Opt. Soc. Am. A 22 (2005) 289.
[13] M. Anguiano-Morales, A. Martinez, M. DavidIturbe-Castillo, S. Chavez-Cerda, Opt. Commun. 281 (2008) 401.
[14] Z. Bouchal, J. Courtial, J. Opt. A: Pure Appl. Opt. 6 (2004) S184.
[15] L.-G. Wang, L.-Q. Wang, S.-Y. Zhu, Opt. Commun. 282 (2009) 1088.
[16] Y. Lin, W. Seka, J.H. Eberly, H. Huang, D.L. Brown, Appl. Opt. 31 (1992) 2708.
[17] C.A. Dartora, M. Zamboni-Racheda, K.Z. Nobrega, E. Recami, H.E. Hernandez-Figueroa, Opt. Commun. 222 (2003) 75.
[18] Methods for Computer Design of Diffractive Optical Elements, in: V.A. Soifer (Ed.), Wiley, New York, 2002, p. 765.
[19] W.-X. Cong, N.-X. Chen, B.-Y. Gu, J. Opt. Soc. Am. A 15 (1998) 2362.
[20] E.R. Dufresne, D.G. Grier, Rev. Sci. Instrum. 69 (1998) 1974.
[21] J.E. Curtis, B.A. Koss, D.G. Grier, Opt. Commun. 207 (2002) 169.
[22] S. Xiang, Numer. Math. 105 (2007) 633;
A. Iserles, S.P. Norsett, Proc. R. Soc. A 461 (2005) 1383.
[23] D. Dayton, S. Sandven, J. Gonglewski, S. Browne, S. Rogers, S. Mcdermott, Opt. Express 1 (1997) 338.
[24] E.J. Fernández, P.M. Prieto, P. Artal, Opt. Express 17 (2009) 11013.